NUCL SCI TECH (2019) 30:109
https://doi.org/10.1007/s41365-019-0626-y

Analysis and optimization of high-power pulse transformer for SXFEL

Yong-Fang Liu[1,2,4] · Hiroshi Matsumoto[3] · Ming Gu[1,4] · Xiao-Xuan Zhou[1,4] · Yong-Hua Wu[1,4] · Zhi-Hao Chen[1,4]

Received: 12 September 2018 / Revised: 18 February 2019 / Accepted: 20 March 2019 / Published online: 5 June 2019

Abstract A C-band accelerator structure was used to accelerate electrons at the Shanghai soft X-ray free-electron laser test facility (SXFEL-TF) in Shanghai Institute of Applied Physics (SINAP). The microwave system of this accelerator structure used a 110 MW pulse modulator and a klystron (PV-5050) to provide the power supply. A pulse transformer is a crucial device in a modulator klystron system and plays significant roles in voltage level transformation, matching impedances, and polarity inversion. This study presents the optimization of a high-voltage pulse transformer. The design considerations of reducing flattop ringing and flattop droop, and shortening leading edge are provided. The model simulation, mechanical design, and the relevant experimental results are also presented.

Keywords Pulse transformer · Pulse modulator · Flattop droop · Leading edge · Flattop ringing

The work was supported by the National Natural Science Foundation of China (No. 11675250).

✉ Yong-Fang Liu
liuyongfang@zjlab.org.cn

✉ Zhi-Hao Chen
chenzhihao@zjlab.org.cn

[1] Shanghai Institute of Applied Physics, Chinese Academy of Sciences, Shanghai 201800, China

[2] University of Chinese Academy of Sciences, Beijing 100049, China

[3] High Energy Accelerator Research Organization, Tsukuba, Ibaraki 3050801, Japan

[4] Shanghai Advanced Research Institute, Chinese Academy of Sciences, Shanghai 201412, China

1 Introduction

An X-ray free-electron laser is regarded as a fourth-generation light source [1–4], with the characteristics of high intensity, exceptional brightness, ultrashort pulse duration, and spatial coherence [5–7]. The Shanghai soft X-ray free-electron laser test facility (SXFEL-TF) requires seven sets of C-band klystrons to provide microwaves with high power [8, 9]. The main specifications of the pulse modulator power supply are a pulse current of 320 A, a pulse voltage of 350 kV, a flattop width of 3 μs, and a repetition rate of 10 Hz [10]. To satisfy the modulator requirements, a durable and dependable high-power pulse transformer with exquisite workmanship is indispensable. The values of design parameters of a C-band pulse transformer are listed in Table 1.

The detailed schematic circuit of the modulator with the pulse transformer is shown in Fig. 1. In this study, the performance parameters of high-voltage pulse transformers in other facilities are investigated [11–13], and a detailed equivalent circuit model of a high-voltage pulse transformer is presented. Based on the analyses of the equivalent circuit model, an optimized design method is also presented. Furthermore, experimentally measured data and waveforms are provided.

2 Pulse transformer modeling

2.1 Equivalent circuit of pulse transformer

In a linear modulator, a pulse transformer is designed as a step-up transformer used for transmitting pulsed power.

Table 1 Values of design parameters of a C-band pulse transformer

Primary side		Secondary side	
Items	Value	Items	Value
Pulse voltage (kV)	22	Pulse voltage (kV)	350
Pulse current (A)	5100	Pulse current (A)	320
Leading edge (μs)	0.5	Leading edge (μs)	0.9
Falling edge (μs)	0.5	Falling edge (μs)	1.2
Flattop (μs)	5.5	Flattop (μs)	3
FWHM (μs)	6	Flattop ripple (%)	0.25
Repetition rate (Hz)	10	Flattop droop (%)	2

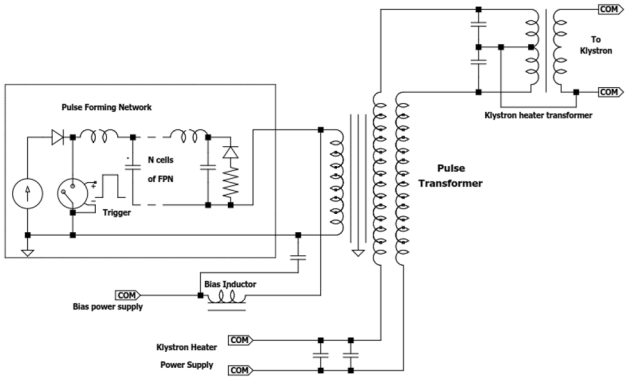

Fig. 1 Detailed circuit of pulse transformer application

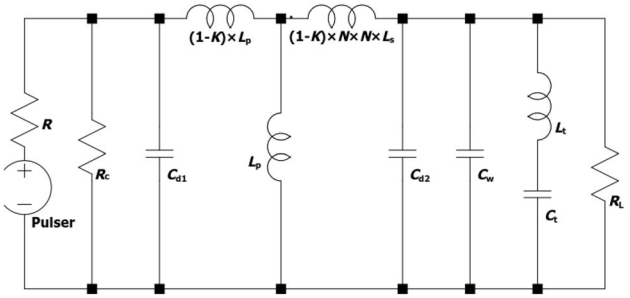

Fig. 2 Equivalent circuit of a typical pulse transformer

We apply a typical equivalent circuit, as presented in Fig. 2, to analyze a pulse transformer.

K denotes the coupling coefficient of the pulse transformer ($K = 1$ in the ideal case), C_{d1} denotes the distributed capacitance of the primary winding line, and C_{d2} denotes the distributed capacitance of the secondary winding line. C_w is the parasitic capacitance between the primary and secondary windings, L_p indicates the primary inductance, L_s indicates the secondary inductance, and R_L indicates the load impedance. N denotes the step-up ratio of the pulse transformer, C_t denotes the parasitic capacitance between the primary winding and ground, and L_t denotes the lead inductance in series with C_t. Table 2 shows a comparison of the main parameters of the C-band pulse transformers in other facilities [14–20].

Table 2 Main parameters of C-band pulse transformers in other facilities

Items	TOSHIBA	SACLA	PAL
Primary inductance (μH)	200	560	600
Leakage inductance (μH)	3	3	2.8
Load capacitance (nF)	–	30	–
Pulse width (μs)	5	5	10
Flattop droop (%)	5.2	1.9	3.1

2.2 Shorten leading edge

In general, we can neglect unrelated parameters, such as L_p, L_t, and C_t, when analyzing the leading edge [21]. In this case, the equivalent circuit for leading edge analysis is shown in Fig. 3. In a line-type modulator, the pulse-forming network (PFN) impedance is usually designed to be equal to the load impedance. The leading edge can be calculated using Eq. (1). This depends on the distributed capacitance and leakage inductance [22].

$$T_r = 2\pi y(\sigma)\sqrt{L_e C_d}, \tag{1}$$

where L_e indicates the leakage inductance, C_d indicates the distributed capacitance, R_L indicates the load impedance, $\sigma = \frac{Z_T}{2R_L}$, and $Z_T = \sqrt{\frac{L_e}{C_d}}$. $y(\sigma)$ depends on the selected damping coefficient σ and is obtained from Table 3.

Figure 4 shows the leading edge for a certain range of σ values. As can be derived from the theories, for a specified value of distributed capacitance, a larger leakage inductance leads to a slower leading edge, and for a certain value of leakage inductance, a small distributed capacitance leads to a smaller overshoot. For instance, in the case of $C_d = 20$ nF and $L_e = 2$ μH, overshoot is approximately 2% compared with the case of $C_d = 30$ nF and $L_e = 2$ μH. The leading edge increases by approximately 200 ns for

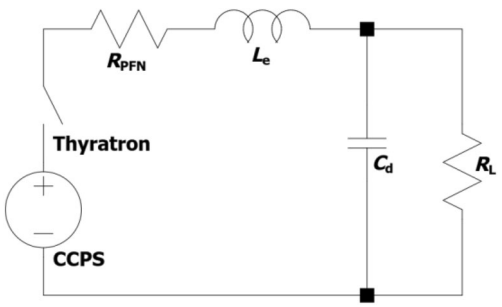

Fig. 3 Equivalent circuit for leading edge analysis

Table 3 Relationship between $y(\sigma)$ and σ

σ	$y(\sigma)$
0.5	0.299
0.6	0.303
0.7	0.311
0.8	0.329
0.9	0.347
1.0	0.374
1.1	0.404
1.2	0.431

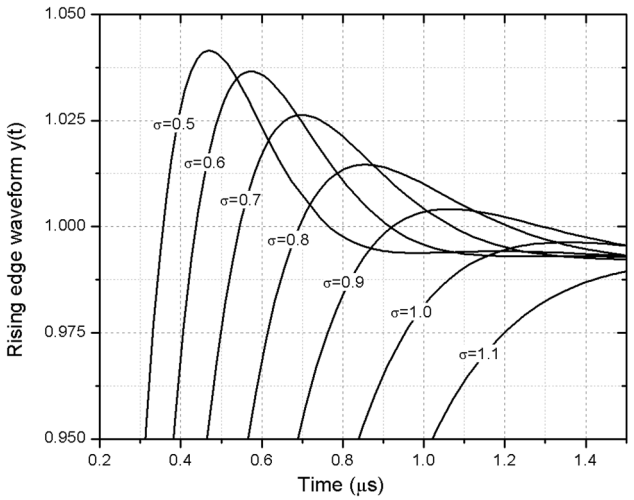

Fig. 4 Leading edge with different values of damping factor σ

C_d = 30 nF and L_e = 3 μH compared with the case of C_d = 30 nF and L_e = 2 μH.

We use Eq. (2) to calculate the leakage inductance. We can also measure it using a precision LCR meter [23].

$$L_e = \frac{\mu_0}{2}\frac{C_L d N_p^2}{L_c}, \tag{2}$$

where μ_0 is the permeability of free space ($4\pi \times 10^{-7}$ H/m), C_L indicates the one-turn mean length of the primary coil, d indicates the distance between the primary and secondary windings, L_c indicates the height of the secondary coil, and N_p indicates the number of primary winding turns.

We can apply corresponding methods to decrease the leakage inductance—for instance, using closed core, cone-shaped windings, and close bifilar winding. The calculated and measured values of leakage inductance of this pulse transformer are 2.25 and 2.3 μH, respectively.

The distributed capacitance includes a stray capacitance between the primary and secondary windings and a stray capacitance in the klystron. The distributed capacitance between the primary and secondary windings can be calculated using Eq. (3). We can also measure the total distributed capacitance using a precision LCR meter.

$$C_d = \frac{2}{3}\frac{\varepsilon_0 \varepsilon_r C_L L_c}{d}(n-1)^2, \tag{3}$$

where ε_0 is the dielectric constant of vacuum, ε_r is the relative dielectric constant, C_L is the one-turn length of the primary winding, L_c is the secondary coil height, n is the transformer ratio, and d is the distance between the primary and secondary windings. The distributed capacitance between the primary and secondary windings is calculated to be 12 nF, and the total distributed capacitance is measured to be 40 nF.

2.3 Flattop droop and primary inductance

Flattop droop depends on the inductance of the primary winding. The equivalent circuit used for flattop droop analysis is shown in Fig. 5. We use Eq. (4) to calculate the voltage across the resistance R_L.

$$U'_L = L_p \frac{di_L}{dt}, \tag{4}$$

where L_p is the primary inductance and i_L is the current flowing through L_p.

Equation (5) can be derived from the principle of Kirchhoff laws.

$$E = U'_L + \left(i_L + \frac{U'_L}{R_L}\right)R_{PFN}, \tag{5}$$

where E is the voltage of the pulse, R_L is the equivalent impedance of klystron in primary side, and R_{PFN} is the PFN characteristic impedance.

The initial conditions (t = 0) are given by Eq. (6):

$$U'_L(t=0) = \frac{R_L E}{R_L + R_{PFN}}. \tag{6}$$

Based on Eqs. (4), (5), and (6), the voltage U'_L can be calculated as follows:

$$U'_L = \alpha E e^{-\frac{t}{T_d}}, \tag{7}$$

where $\alpha = \frac{R_L}{R_L + R_{PFN}}$ is called the transmission factor from the primary to secondary windings of the pulse transformer and

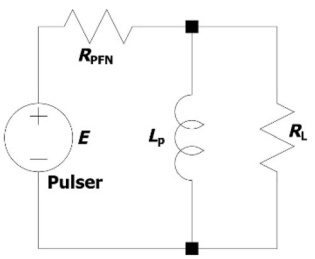

Fig. 5 Equivalent circuit for flattop droop analysis

$T_d = \frac{L_p(R_L+R_{PFN})}{R_L R_{PFN}}$ is called the time constant of the pulse transformer.

The flattop droop D is defined in Eq. (8):

$$D = 1 - e^{-\frac{t}{T_d}}. \tag{8}$$

In a linear modulator, we usually design the PFN output impedance to be matched to the load impedance. The flattop droop D is determined by the primary inductance, where the relationship between primary inductance and flattop droop is given in Eq. (9).

$$L_p = \frac{tR_L R_{PFN}}{(R_L + R_{PFN})\ln\left(\frac{1}{1-D}\right)} \approx \frac{tR_L R_{PFN}}{(R_L + R_{PFN})D} \tag{9}$$

Figure 6 shows the primary inductance versus flattop droop for the C-band klystron pulse transformer. Figure 7 presents a graphical view of flattop droop with different values of primary inductance in the simulation of the C-band pulse transformer. As shown in Fig. 7, a primary inductance of 100 μH results in approximately 10.8% flattop droop, a primary inductance of 300 μH results in approximately 3.6% flattop droop, and a primary inductance of 500 μH only results in approximately 2.2% flattop droop.

The primary inductance is associated with the core material permeability, winding turns, core size, and magnet flux pass length [24]. It can be calculated using Eq. (10):

$$L_p = u_0 \times u_r \times N_p^2 \times \frac{A_{core}}{l_m}, \tag{10}$$

where μ_0 is the permeability of free space ($4\pi \times 10^{-7}$ H/m), u_r is the permeability of the core material, l_m is the average magnetic pass length, A_{core} is the core cross-sectional area, and N_p is the number of primary winding turns.

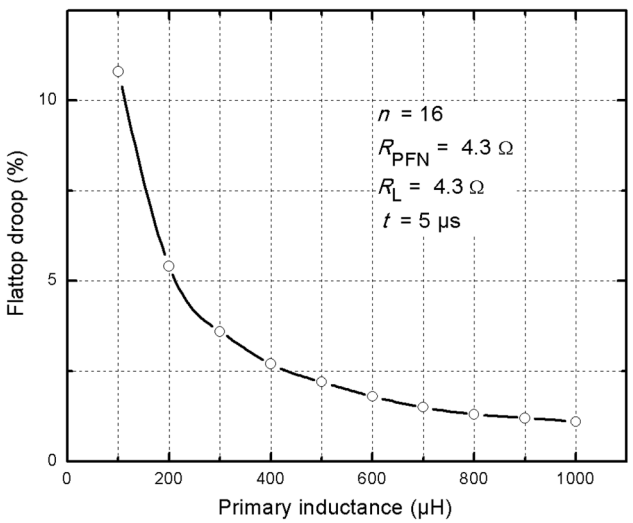

Fig. 6 Primary inductance versus flattop droop

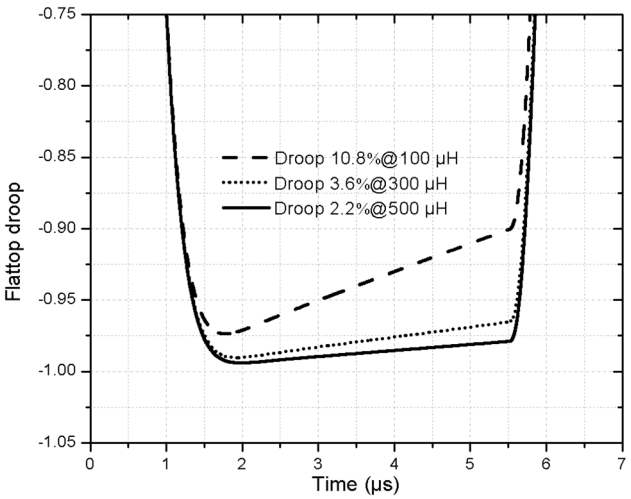

Fig. 7 Simulation result of flattop droop with different values of primary inductance

In general, core materials with high permeability are preferred. High permeability ensures the fewest turns to attain our desired magnetizing inductance [25]. Fewer turns lead to lower leakage inductance, smaller distributed capacitance, and smaller winding resistance. Silicon steel and ferrite are the most commonly used materials for the design of a high-power pulse transformer core. In our design, the primary inductance is 226 μH. Thus, we can calculate the flattop droop as 5%.

2.4 Reducing flattop ringing

Flattop ringing is determined by the parasitic capacitance between the primarily coil and ground C_t and the lead inductance L_t in series with C_t. Figure 8 shows the circuit used to analyze the flattop ringing. Figure 9 shows the flattop ringing with different values of L_t and C_t. The ringing frequency can be calculated using Eq. (11).

$$F\,[\mathrm{Hz}] = \frac{1}{2\pi\sqrt{L_t C_t}} \tag{11}$$

In summary, the main parameters of the C-band high-power pulse transformer are listed in Table 4.

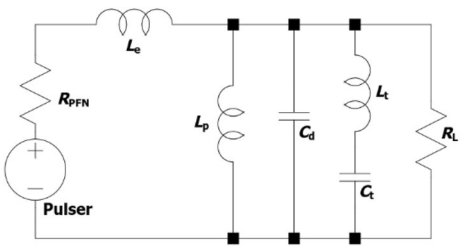

Fig. 8 Equivalent circuit for analyzing flattop ringing

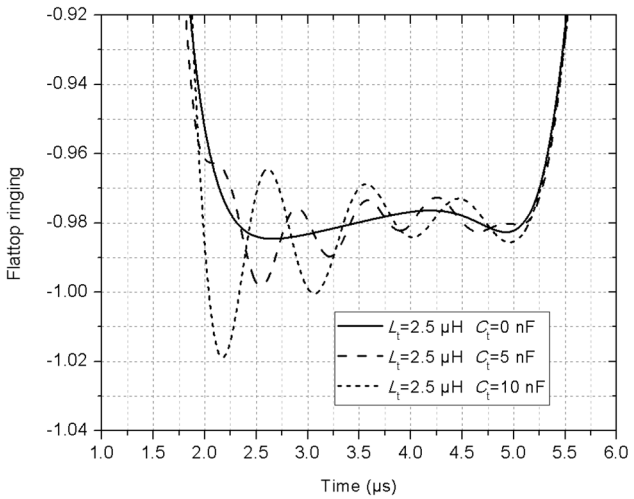

Fig. 9 Flattop ringing with different values of L_t and C_t

Table 4 Main parameters of the C-band high-power pulse transformer

Items	Value
Primary inductance (μH)	226
Secondary inductance (mH)	58.50
Leakage inductance (μH)	2.3
Primary impedance (mΩ)	3.9
Secondary impedance (mΩ)	1031
Load capacitance (nF)	40
Parasitic capacitance between the core and secondary coil (pF)	136
Parasitic capacitance between the primary and secondary coils (pF)	140

3 Mechanical design

Using parameter analysis, we optimize and fabricate the pulse transformer. Figure 10 shows the geometrical structure of the pulse transformer. The transformer is designed to have two secondary windings. To reduce the distributed coupling parameters and reduce the risk of flashover, the insulation distances between primary coil and secondary coil are increased between the input and output points. The transformer core shape is almost rectangular, apart from the corners, which are rounded. The cores are made of silicon steel sheet with high permeability. The primary winding is composed of two coils in parallel, each having six turns. The secondary winding of the transformer consists of 96 turns.

4 Test results and discussion

The pulse transformer is installed in a metallic tank filled with condenser oil, which is used as a coolant and insulator. Figure 11 shows a picture of the klystron and oil tank with the pulse transformer inside. After the system was installed, an experimental test was performed. Figure 12 presents the typical measured waveforms with a klystron load: One illustrates the pulse current obtained using a precise pulsed current sensor (0.1 V/A) and the other illustrates the pulse voltage measured using a high-voltage divider (9300:1). Table 5 summarizes the test parameters of the typical measured waveforms of the C-band high-power pulse transformer.

Based on our model analysis in this study, L_e = 2.3 μH, $C_d = 40\,\text{nF}$, $Z_T = \sqrt{\frac{L_e}{C_d}} = 7.58\,\Omega$, and $R_L = \frac{V_p}{I_p \times n^2} = \frac{380\,\text{kV}}{368\,\text{A} \times 16^2} = 4.03\,\Omega$, where V_p is pulse voltage of the klystron, I_p is pulse current of the klystron, and n is the

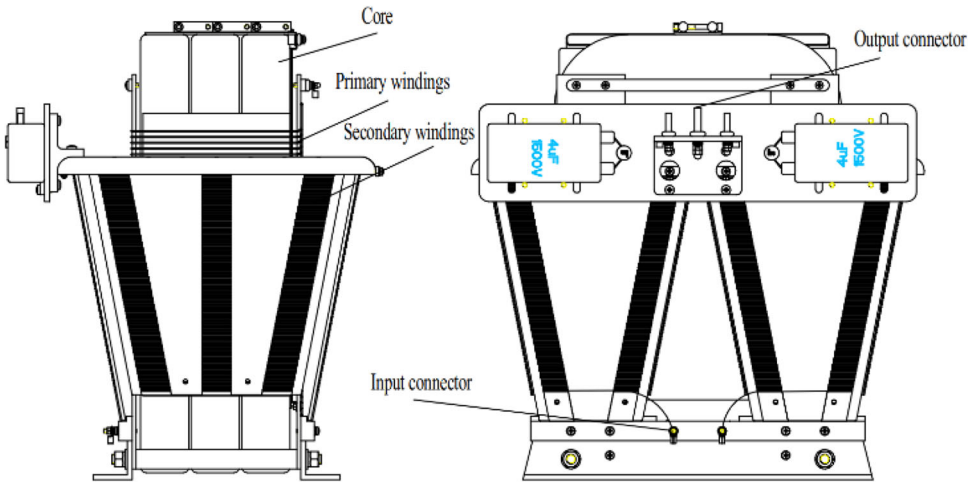

Fig. 10 Geometrical structure of the pulse transformer

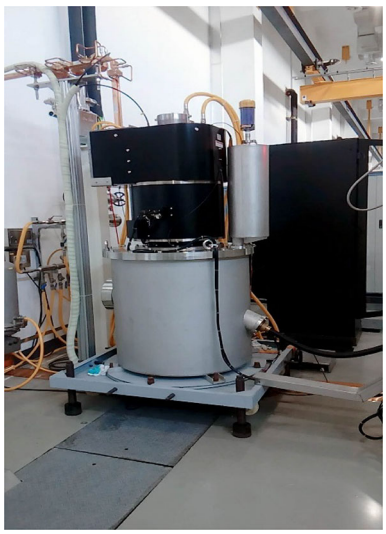

Fig. 11 Klystron and pulse transformer oil tank

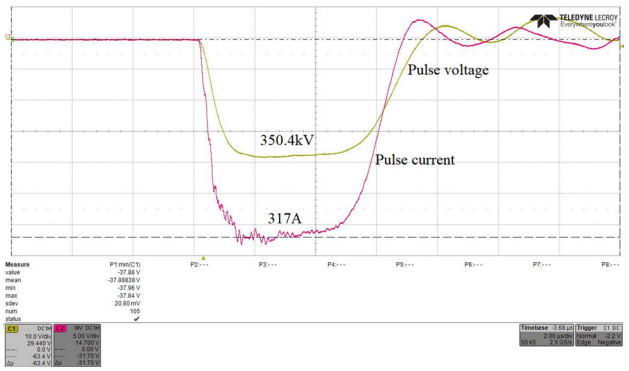

Fig. 12 Output waveforms

Table 5 Test parameters of the pulse transformer waveform

Items	Value	Items	Value
Pulse voltage (kV)	350	Pulse current (A)	317
Leading edge (ns)	746	Falling edge (μs)	1.3
Flattop (μs)	3.1	FWHM (μs)	5.6

transformer ratio. Thus, $\sigma = \frac{Z_T}{2R_L} = 0.95$ and $y(\sigma) = 0.36$. We can calculate the leading edge as $T_r = 686\,\text{ns}$ using Eq. (1). The experimentally obtained leading edge is 746 ns as shown in Fig. 13. The increase in the measured value over the theoretical expected value is due to the increased distributed capacitance after installation in the oil tank.

Our work aims to elaborate the analysis of a pulse transformer by using a circuit model. Using this circuit model, we can determine the relationship between the distribution parameters of the pulse transformer and the output pulse shape. The analysis of the circuit model shows how to obtain a shorter leading edge, smaller flattop ringing, and smaller flattop droop. The results can be used to guide mechanical design to obtain appropriate circuit parameters.

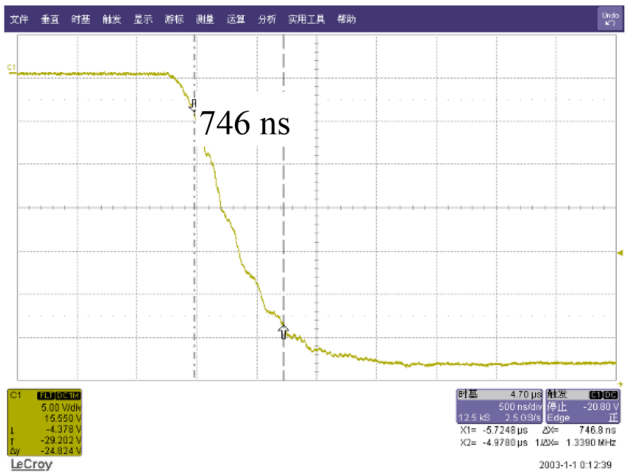

Fig. 13 Measurement result of leading edge

5 Conclusion

A pulse transformer as a primary device in a high-gradient accelerating structure has been studied in the Shanghai Institute of Applied Physics. A detailed equivalent circuit modeling a high-power pulse transformer was presented, especially for shortening the leading edge and reducing the flattop ringing and droop. Subsequently, its validity was confirmed using LTspice code and through experiment using the SXFEL high-power microwave system. The results obtained from the experiments and theoretical analysis were compared. Based on the circuit analysis, we optimized our mechanical design. It was indicated by relevant test results that this C-band high-power pulse transformer satisfied the requirements of a practical target. The circuit models and analysis methodology can be applied in the research and development of future high-power pulse transformers.

References

1. M. Altarelli, From 3rd to 4th generation light sources: free electron lasers in the X-ray range. J. Crystallogr. Rep. **55**, 1145–1151 (2010). https://doi.org/10.1134/S1063774510070072
2. C. Feng, H.X. Deng, Review of fully coherent free-electron lasers. Nucl. Sci. Tech. **29**(11), 160 (2018). https://doi.org/10.1007/s41365-018-0490-1
3. Z.T. Zhao, C. Feng, K.Q. Zhang, Two-stage EEHG for coherent hard X-ray generation based on a superconducting linac. Nucl. Sci. Tech. **28**, 117 (2017). https://doi.org/10.1007/s41365-017-0258-z

4. T. Phimsen, B.C. Jiang, H.T. Hou et al., Improving Touschek lifetime and synchrotron frequency spread by passive harmonic cavity in the storage ring of SSRF. Nucl. Sci. Tech. **28**(8), 108 (2017). https://doi.org/10.1007/s41365-017-0259-y
5. Z. Zhao, D. Wang, Q. Gu et al., Status of the SXFEL facility. Appl. Sci. **7**, 607 (2017). https://doi.org/10.3390/app7060607
6. Z. Wang, C. Feng, Q. Gu et al., Generation of double pulses at the Shanghai soft X-ray free electron laser facility. Nucl. Sci. Tech. **28**, 28 (2017). https://doi.org/10.1007/s41365-017-0188-9
7. C.H. Miao, M. Liu, C.X. Yin et al., Precise magnetic field control of the scanning magnets for the APTRON beam delivery system. Nucl. Sci. Tech. **28**, 172 (2017). https://doi.org/10.1007/s41365-017-0324-6
8. Z.T. Zhao, D. Wang, L.X. Yin et al., The current status of the SXFEL project. AAPPS Bull. **26**, 12–24 (2016). https://doi.org/10.22661/AAPPSBL.2016.26.1.12
9. W. Fang, Q. Gu, Z. Zhao et al., R&D of new c-band accelerating structure for SXFEL facility. Paper presented at the 4th international particle accelerator conference, Shanghai, 12–17 May 2013
10. C. Wang, W. Fang, D. Chun, Design and study of a C-band pulse compressor for the SXFEL linac. Nucl. Sci. Tech. **25**, 020101 (2014). https://doi.org/10.13538/j.1001-8042/nst.25.020101
11. Z. Zhang, X. Tan, Review of high power pulse transformer design. J. Phys. Procedia **32**, 566–574 (2012). https://doi.org/10.1016/j.phpro.2012.03.602
12. S. Candolfi, P. Viarouge, D. Aguglia et al., Hybrid design optimization of high voltage pulse transformers for klystron modulators. J. IEEE Trans. Dielectr. Electr. Insul. **22**, 3617–3624 (2016). https://doi.org/10.1109/TDEI.2015.005047
13. S. Blume, M. Jaritz, J. Biela, Design and optimization procedure for high voltage pulse power transformers. IEEE Trans. Plasma Sci. **43**, 3385–3391 (2015). https://doi.org/10.1109/TPS.2015.2448351
14. A. Baktash, A. Vahedi, Design of a wound core pulse transformer using multiobjective optimization method. IEEE Trans. Plasma Sci. **43**, 857–863 (2015). https://doi.org/10.1109/TPS.2015.2394478
15. Z. Zhang, H. Yang, J. Yang et al., Compact megavolt pulse transformer with inner magnetic core and conical secondary windings, in *2015 IEEE Pulsed Power Conference, Austin*. https://doi.org/10.1109/ppc.2015.7296978
16. D. Bortis, G. Ortiz, J.W. Kolar, Design procedure for compact pulse transformers with rectangular pulse shape and fast rise times. J. IEEE Trans. Dielectr. Electr. Insul. **18**, 1171–1180 (2011). https://doi.org/10.1109/TDEI.2011.5976112
17. Y. Wang, M. Li, K. Li et al., Optimal design and experimental study of pulse transformers with fast rise time and large pulse duration. IEEE Trans. Plasma Sci. **42**, 300–306 (2014). https://doi.org/10.1109/TPS.2013.2295280
18. S. Candolfi, S. Blume,D. Aguglia et al., Evaluation of insulation systems for the optimal design of high voltage pulse transformers, in *2014 IEEE International Power Modulator and High Voltage Conference, Santa Fe, New Mexico*. https://doi.org/10.1109/ipmhvc.2014.7287336
19. F. Pan, L. Jin, P. Pan et al., Design procedure of the leakage inductance for a pulse transformer considering winding structures. J. IEEE Trans Plasma Sci. **45**, 2504–2510 (2017). https://doi.org/10.1109/TPS.2017.2732163
20. J.S. Oh, M.H. Cho, W. Namkung et al., Rise time analysis of pulsed klystron-modulator for efficiency improvement of linear colliders. J. Nucl. Inst. Methods Phys. Res. A **443**, 223–230 (2000). https://doi.org/10.1016/s0168-9002(99)01171-7
21. W. Zhao, X.Q. Guo, W. Chen et al., Temporal characteristic analysis of single event effects in pulse width modulator. Nucl. Sci. Tech. **28**, 92 (2017). https://doi.org/10.1007/s41365-017-0254-3
22. B. Yang, L. Cao, J. Yang et al., Equivalent circuit model for the insulated core transformer. Nucl. Sci. Tech. **27**, 68 (2016). https://doi.org/10.1007/s41365-016-0060-3
23. J.J. Tian, Y.H. Liu, R. Li et al., Magnetic flux leakage analysis and compensation of high-frequency planar insulated core transformer. Nucl. Sci. Tech. **26**, 030105 (2015). https://doi.org/10.13538/j.1001-8042/nst.26.030105
24. Z. Benesova, V. Kotlan, New approach to surge phenomena analysis in transformer winding, in *2014 IEEE International Power Modulator and High Voltage Conference, Santa Fe, New Mexico*. https://doi.org/10.1109/ipmhvc.2014.7287259
25. D. Habibinia, M. Feyzi, Optimal winding design of a pulse transformer considering parasitic capacitance effect to reach best rise time and overshoot. IEEE Trans. Dielectr. Electr. Insul. **21**, 1350–1359 (2014). https://doi.org/10.1109/TDEI.2014.6832283